ACS APPLIED ENGINEERING MATERIALS

pubs.acs.org/acsaenm Article

Carbon-Sequestration Straw Cellulose-Aerogel Gradient Thermal Insulation Material

Arpita Sarkar, Pratyush Kumar Singh, Long Zhu, Danial Faghihi, and Shenqiang Ren*

Cite This: https://doi.org/10.1021/acsaenm.3c00664 Read Online

ABSTRACT: Green superinsulation materials are essential for net-zero sustainable building envelopes. Realizing such potential is indispensable for simultaneously achieving carbon-sequestration and superinsulation performance. Here, we report the synthesis of a water glass-based silica aerogel exhibiting a thermal conductivity of 17.2 mW/m·K and a high porosity of 92%. We used carbon-sequestration wheat straw fiber to create a gradient cellulose-aerogel composite to improve mechanical stability. The as-prepared gradient composite exhibits a thermal conductivity of 27.1 mW/m·K and a flexural modulus of 824 MPa, while exhibiting superhydrophobicity (water contact angle of 135.4°) for the development of green building insulation materials.

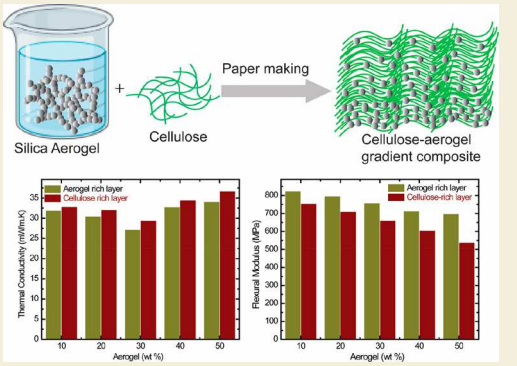

KEYWORDS: *Wheat straw, silica aerogel, cellulose aerogel gradient composites, thermal insulation, carbon-sequestration*

INTRODUCTION

Wheat straw, a readily available agricultural waste product, has recently gained substantial recognition for its potential to mitigate carbon emissions within the construction industry.[1−4] This versatile crop residue, remaining in abundance after the wheat harvest, emerges as a sustainable and environmentally friendly resource for the sequestration of carbon dioxide, a prominent contributor to the ongoing challenge of climate change. Furthermore, the incorporation of agricultural wheat straw into aerogel materials has shown significant promise.[5,6] In this context, wheat straw's cellulose network plays a pivotal role in enhancing the mechanical strength and durability of aerogel/cellulose composites, while the aerogel itself serves as the primary agent in lowering the thermal conductivity of these innovative materials.[7,8] This synergy between wheat straw and aerogel opens up new avenues for the development of thermal insulation materials that are not only eco-friendly but also highly efficient in reducing heat transfer. As we continue to seek sustainable solutions to combat climate change and promote environmental responsibility, the utilization of wheat straw in conjunction with advanced materials like aerogel represents a compelling step forward in addressing the multifaceted challenges of our times.

In this study, we report the incorporation of wheat straw-derived cellulose into silica aerogel for the preparation of gradient cellulose−aerogel composites to improve the mechanical strength of the materials. The preparation of silica aerogels via ambient pressure drying is demonstrated using sodium silicate (water glass). Additionally, we investigate the roles of sodium dodecyl sulfate, sodium bicarbonate, and mesitylene in enhancing the porosity and thermal insulation of as-grown silica aerogels. The as-prepared gradient composite shows low thermal conductivity (27.1 mW/m·K), mechanical strength (824 MPa), and hydrophobicity (water contact angle of 135.4°). This eco-friendly and cost-effective synthesis method holds promise for the production of silica aerogels and gradient cellulose-aerogel composites with low thermal conductivity and high mechanical strength.

RESULTS AND DISCUSSION

Aerogel is a highly porous and ultralight material, renowned for its unique characteristics, including low density (<0.05 g/cm^3), high porosity (>80%), low dielectric constant (∼1−2), and ultralow thermal conductivity (<0.02 W/m·K).[9−13] However, silica aerogels are fragile,[14] and recent studies have shown that the presence of a fibrous network in aerogels reduces the formation of "necks" in the skeleton, thus enhancing its mechanical stability.[15−17] Figure 1a shows the schematic diagram of the synthesis of sodium silicate-based silica aerogels. Surfactants play a key role in improving the porosity and reducing the thermal conductivity of silica aerogels. In the synthesis of water glass-based silica aerogel, the anionic

Received: October 29, 2023
Revised: December 18, 2023
Accepted: December 19, 2023

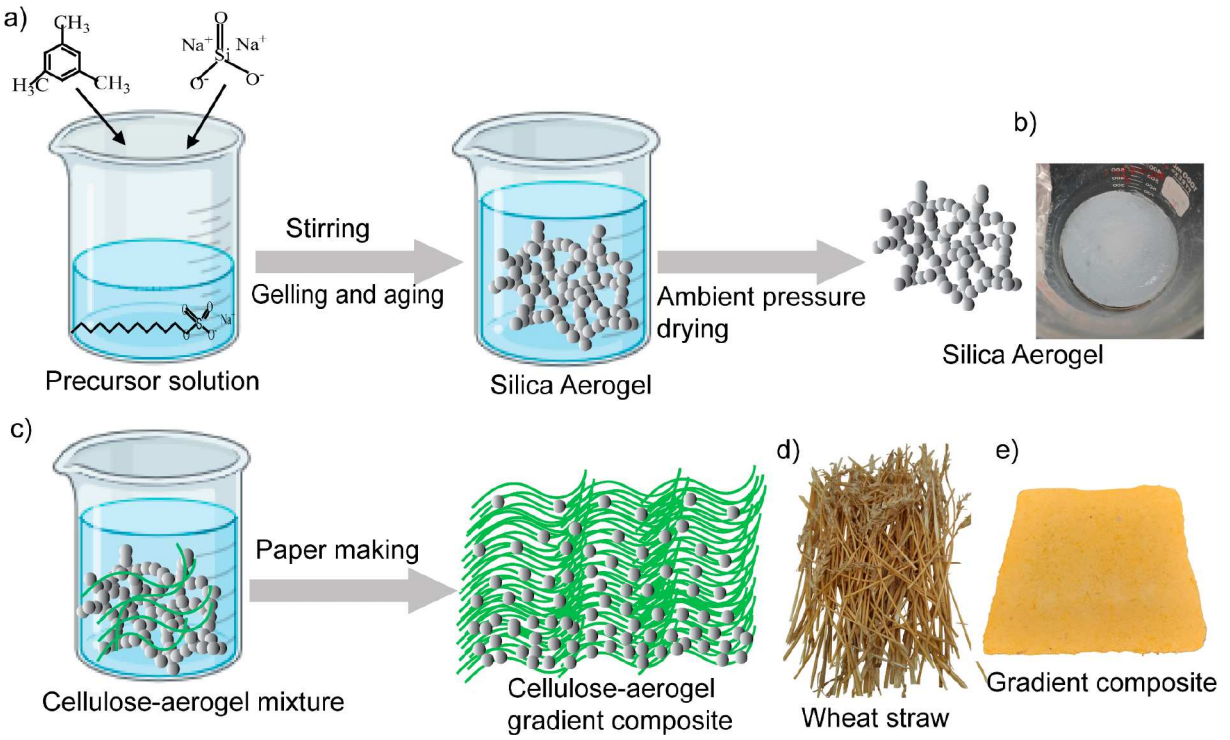

Figure 1. (a) Schematic diagram of the synthesis of water glass-based silica aerogel, (b) image of synthesized silica aerogel. (c) Schematic diagram of the synthesis of gradient cellulose-aerogel composite, (d) image of raw wheat straw, and (e) image of gradient cellulose-aerogel composite (30 wt %).

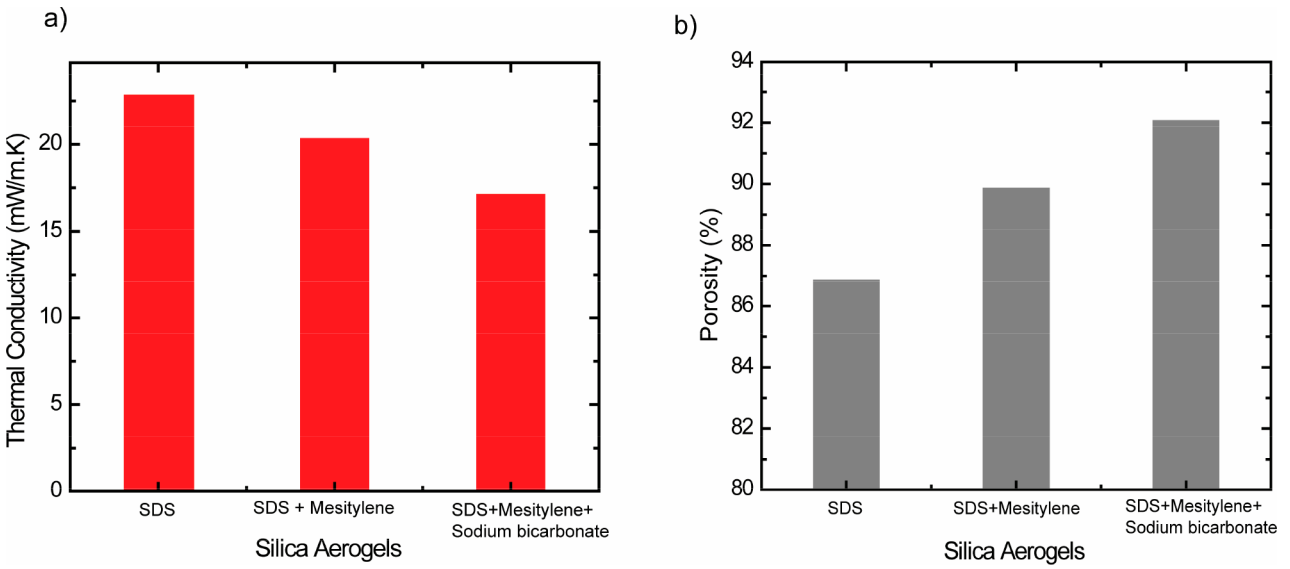

Figure 2. (a) Thermal conductivity of different waterglass-based aerogel. (b) Porosity of different water−glass based aerogel.

surfactant sodium dodecyl sulfate (SDS) serves as a templating agent to prevent the collapse of the mesoporous structure during gelation and drying. Moreover, mesitylene and sodium bicarbonate improve the overall porosity of silica aerogels. Figures 1b and S1 show the images of the waterglass-based silica aerogel, demonstrating the successful gel formation. Figure 1c illustrates the schematic diagram of the fabrication of gradient cellulose−aerogel composite from the mixture of water glass-based silica aerogel and sodium hydroxide pretreated wheat straw fiber. During the fabrication of cellulose-aerogel composite smaller aerogel particles settle at the bottom using a papermaking setup, creating a gradient structure with a higher aerogel concentration on the lower side of the composite. Figures 1d, S2, and 1e display images of the raw wheat straw, sodium hydroxide-treated wheat straw, and the gradient cellulose-aerogel composite, respectively. After blending, sodium hydroxide treatment, and drying, the long wheat straw becomes shorter (Figure S2a). The gradient composite exhibits excellent shape and uniformity (Figure 1e and Figure S2b).

Figure 2a shows the thermal conductivity of the as-prepared silica aerogels. The thermal conductivity of SDS templated

https://doi.org/10.1021/acsaenm.3c00664
ACS Appl. Eng. Mater. XXXX, XXX, XXX−XXX

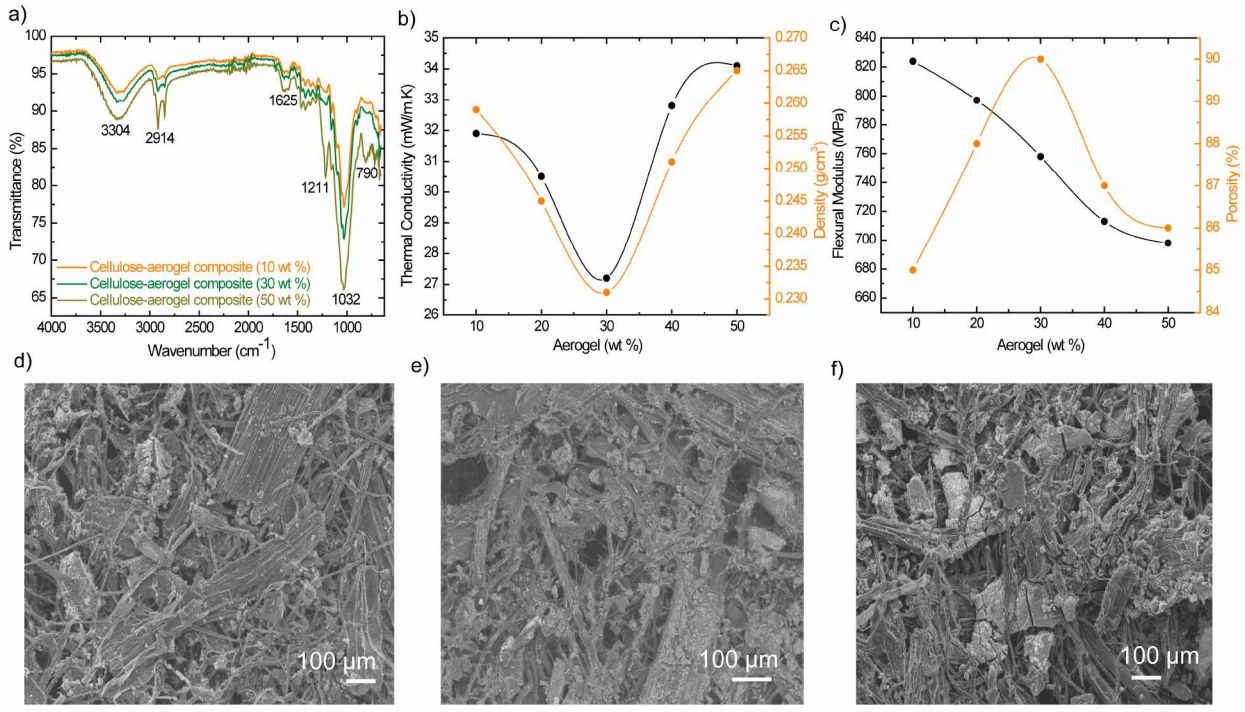

Figure 3. (a) FTIR spectra of gradient cellulose−aerogel composites with different aerogel wt %. (b) Plot of thermal conductivity vs aerogel wt % for the gradient composite. (c) Plot of flexural modulus vs aerogel wt % for the gradient composite. (d−f) SEM images of the gradient cellulose−aerogel composite with different aerogel wt % of (d) 10, (e) 30, and (f) 50 wt %.

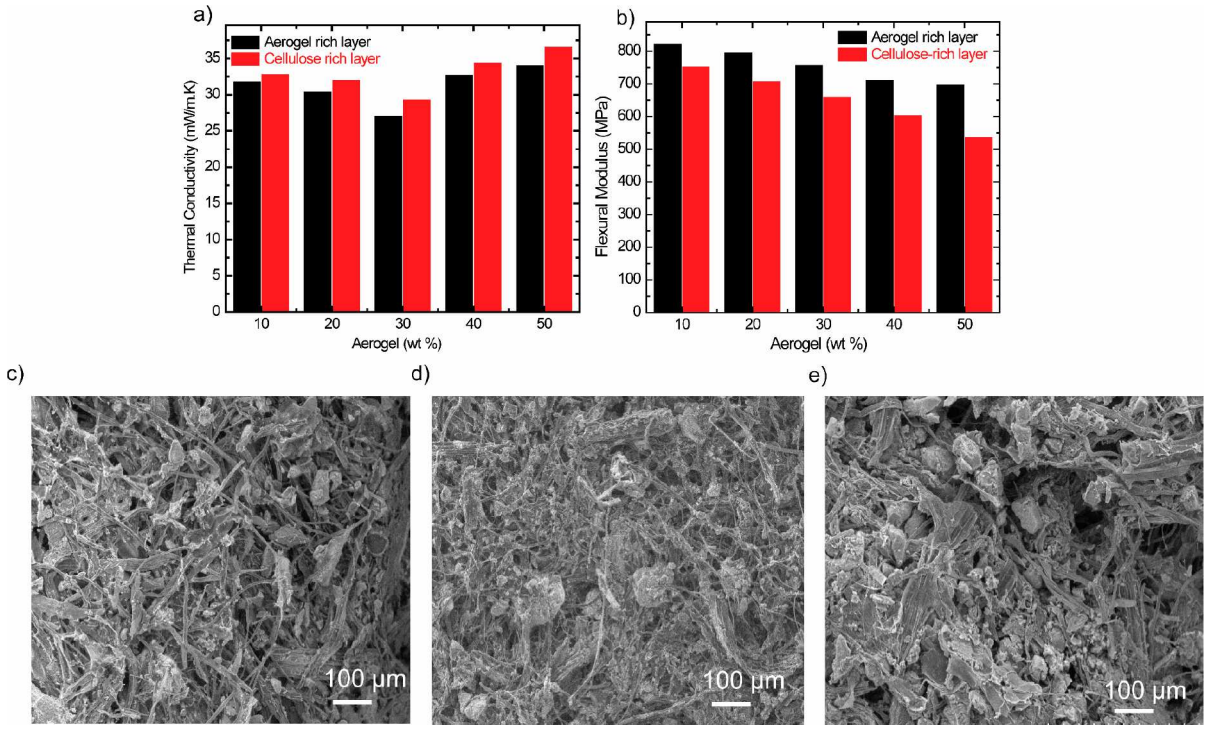

Figure 4. (a) Thermal conductivity change between different layers of gradient composite. (b) Flexural modulus change between different layers of gradient composite. (c−e) SEM images of (c) cellulose-rich layer, (d) intermediate layer, and (d) aerogel-rich layer of gradient composite, respectively.

silica aerogel (SA1) is 22.9 mW/m·K. On the other hand, in the case of SDS and mesitylene-templated silica aerogel (SA2), the thermal conductivity decreased to 20.4 mW/m·K. Moreover, adding sodium bicarbonate along with SDS and mesitylene (SR3) further decreases the thermal conductivity to 17.2 mW/m·K. This indicates that sodium bicarbonate and mesitylene play an important role in lowering thermal conductivity of the silica aerogels. To investigate the

https://doi.org/10.1021/acsaenm.3c00664
ACS Appl. Eng. Mater. XXXX, XXX, XXX−XXX

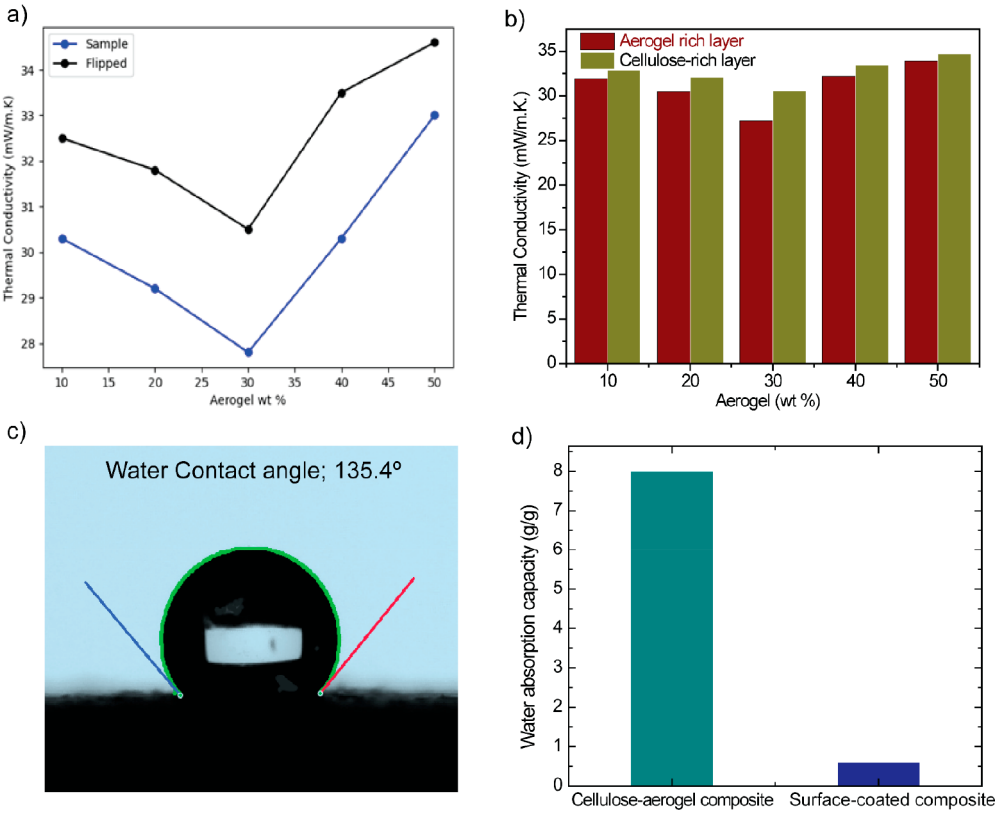

Figure 5. Thermal conductivity for five samples with different aerogel wt % for both the original sample and the flipped composites: (a) finite element results, (b) experimental results, (c) water contact angle of surface-coated gradient composite. (d) Change in water absorption capacity of coated and uncoated coated gradient composite.

underlying reason for this, we conducted additional characterizations of the porosity of the prepared aerogels. Figure 2b reveals the porosity of the as-prepared silica aerogels. The porosity of SA1, SA2, and SA3 is 87%, 90%, and 92%, respectively, supporting the enhanced porosity in the case of sodium bicarbonate and mesitylene-based silica aerogel.

As the thermal conductivity for SA3 is lower than that of SA1 and SA2, we prepared a gradient cellulose aerogel composite from the mixture of SA3 and sodium hydroxide-treated straw fiber to improve the composite's mechanical stability (Figure S3). Figure 3a displays the Fourier-transform infrared spectroscopy (FTIR) spectra of the different ratios of the gradient cellulose aerogel composites. All the FTIR spectra show a typical set of peaks for lignocellulose such as 3304 cm^{-1} (O−H stretching vibrations), 2914 cm^{-1} (C−H stretching vibration), 1625 cm^{-1} (bending vibration of C═O), and 1032 cm^{-1} (bending vibration of C−O−C). Moreover, a peak appeared for Si−O−Si bonds at 790 cm^{-1} with increasing aerogel concentration indicating the presence of SiO_2 in the gradient composite. Figure 3b reveals the thermal conductivity change with increasing aerogel concentration in the gradient composites. At first, the thermal conductivity of the gradient composites decreases from 32 to 27.1 mW/m·K with increasing aerogel concentration from 10 to 30 wt % due to the increased porosity and low density of the composites. However, increasing the aerogel concentration above 30 wt % leads to the aggregation of the aerogel particles into the gradient composites, which results in increased thermal conductivity due to increased density. The thermal conductivity for the 40 and 50 wt % gradient composites are 32.8 and 34.1 mW/m·K, respectively. The flexural modulus of the gradient composites is shown in Figure 3c and decreases with increasing aerogel concentration from 10 to 30 wt % due to the increase in its porosity. The optimum thermal conductivity and flexural modulus of the as-prepared gradient composite are found to be 27.1 mW/m·K and 824 MPa, respectively. Figures 3d−f and S4 show the scanning electron microscopy (SEM) images of the different aerogel wt % of the gradient composites which clearly reveal the aggregation of aerogel particles in the case of 40 and 50 wt % composites.

Due to the gradient characteristics, the thermal conductivity and flexural modulus of the gradient composite show an orientation dependence behavior as shown in Figure 4a,b. Gradient characteristics allow the aerogel particles to accumulate in the bottom layer of the composite. When the heat flows occur through the aerogel-rich side it results in lower thermal conductivity. Figure 4a displays the difference in thermal conductivity between the aerogel-rich layer and the cellulose-rich layer which is around 1.8−2.3 mW/m·K. Similar phenomena have been observed in the case of flexural modulus. From Figure 4b it is clear that the aerogel-rich layer shows higher flexural modulus than the cellulose-rich layer of the gradient composite. A visible difference in flexural modulus (80−120 MPa) has been observed between the aerogel-rich layer and the cellulose-rich layer, which further supports the gradient characteristics of the composites. Figure 4c−e shows the SEM images of the cellulose-rich layer, intermediate layer, and aerogel-rich layer of 30 wt % gradient composite, confirming the gradient distribution of the aerogel particles along the depth of the composite.

Furthermore, the thermal behavior of aerogel−cellulose composite has been studied via a finite element model which

https://doi.org/10.1021/acsaenm.3c00664
ACS Appl. Eng. Mater. XXXX, XXX, XXX−XXX

accounts for varying aerogel concentration through thickness. To compare the finite element results with the experimental observations, we compute the thermal conductivity of the composite using the average solid and fluid temperature flux through the material. Figure 5a shows the thermal conductivity computed through the thermal model for both the original sample and the flipped sample. The variation of thermal conductivity with aerogel wt % from the finite element model is nearly similar to the results obtained from the experiments (Figure 5b). The finite element simulations in this work rely on the multiphase heat transfer and mechanical models[18] developed based on the continuum theory of mixture. The governing equations of the heat-transfer model at steady-state condition can be written as follows.

$$-\nabla\cdot(\phi_s\kappa_s\nabla\theta_s) = -h(\theta_s - \theta_f)$$

$$-\nabla\cdot(\phi_f\kappa_f\nabla\theta_f) = +h(\theta_s - \theta_f)$$

In these equations θ_s and θ_f are the solid and gaseous temperatures, κ_s = 33.5 mW/m·K and κ_f = 0.08 mW/m·K are the conduction coefficient of solid and gaseous phases, and $h > 0$ is called interstitial coefficient accounting for the interactions among solid and fluid temperatures. The volume fraction of the gaseous phase is described by ϕ_f (porosity) and the combined volume fractions of the fibers and aerogel (solid phase) by ϕ_s, such that $\phi_f + \phi_s = 1$. To model the experimental thermal measurements, we consider a rectangular domain of the aerogel composite with length 70 mm and width 140 mm and impose convective boundary conditions at the top and bottom surfaces

$$k_s\nabla\theta = h_{air}(\theta - \theta_{cold}),\ k_s\nabla\theta = h_{air}(\theta - \theta_{hot})$$

where θ_{hot} = 308.5 K and θ_{cold} = 288.5 K are the ambient temperatures. In our numerical simulations, we explored two scenarios involving gradient porosity distributions across the thickness of the sample. In the first scenario, the highest concentration of aerogel was positioned at the bottom of the sample. This distribution was represented by a linearly varying porosity ranging from 0.9 at the top to a range of 0.8−0.88. In the second scenario (i.e., flipped sample), the aerogel concentration was reversed, with the highest concentration now situated at the top of the sample. In addition, we compute the flexural modulus of the composite using the average stress and strain through the material.[18]

Moreover, we have also studied the flexural modulus computed through the mechanical model for both the original sample and the flipped sample (Figures S5 and S6). The finite element simulations are based on the multiphase mechanical models proposed in ref 18. For modeling three-point bending, we consider a static condition. Additionally, since gas is trapped in the pore, we assume low permeability of the composite with respect to gas flux. The governing equations of the multiphase mechanical model[18] can be written as

$$-\nabla\cdot\sigma = 0$$

$$\sigma = \lambda tr(\epsilon)I + 2\mu\epsilon$$

$$\epsilon = \frac{1}{2}(\nabla u + (\nabla u)^T)$$

where $\boldsymbol{\sigma}$ is the stress in the solid phase, λ and μ are Lame's elasticity parameters of the composite, $\boldsymbol{I}$ is the identity tensor, $tr(\cdot)$ is the trace operator, $\boldsymbol{\epsilon}$ is the solid strain, and $\boldsymbol{u}$ is the solid displacement. The compressibility effect of the gaseous phase (i.e., pore pressure) is viewed as dependency of the elastic parameters to porosity, such that

$$\lambda = \lambda_s - \frac{2\phi_f - 1}{\phi_f}K_f;\ \mu = \mu_s$$

where λ_s and μ_s are the elasticity parameters of the solid phase, and the constant K_f is the bulk modulus of the air (fluid phase). The values for the parameters are λ_s = 480 MPa, μ = 305 MPa, and K_f = 0.142 MPa.

The dirichlet boundary conditions with zero displacement have been applied at the two points A and B and a point load has been applied at the point C on the top surface as shown in Figure S5. In the first scenario, the highest concentration of aerogel was positioned at the bottom of the sample. This distribution was represented by a linearly varying porosity ranging from 0.9 at the top to a range of 0.8−0.88. In the second scenario (i.e., flipped sample), the aerogel concentration was reversed, with the highest concentration now situated at the top of the sample. Figure S6 shows the variation of elastic modulus with aerogel wt % from the finite element model is closely similar to the results obtained from the three-point bending experiments.

Furthermore, water absorption capability and hydrophobicity are the key factors for building insulation materials. The wettability of trimethylchlorosilane (TMCS)-treated gradient composite has been studied by water contact angle measurements and is shown in Figure 5c. Figure 5c reveals the water contact angle of TMCS surface-coated gradient composite is 135.4°, which indicates the super hydrophobicity of the coated gradient composite after surface treatment. Moreover, the water absorption capacity of the coated gradient composite is 8 times lower than the pristine composite (Figure 5d), which implies surface treatment has significantly improved the hydrophobicity of the gradient composite.

CONCLUSION

In this study, we have synthesized water glass-based silica aerogels using ambient pressure drying. The surfactants and additives improve the porosity and decrease the thermal conductivity of as-grown silica aerogels. Moreover, to improve the mechanical stability of the material, we have prepared a gradient cellulose−aerogel composite which shows excellent low thermal conductivity along with mechanical strength and superhydrophobicity. The gradient characteristics and thermal behavior of the composite have been also studied via a finite element model which accounts for varying aerogel concentration through thickness. The as-prepared silica aerogels and gradient composite show a promising way for the development of future thermal insulation materials.

EXPERIMENTAL SECTION

Materials

Sodium dodecyl sulfate (SDS), mesitylene, and water glass were purchased from Sigma-Aldrich. Wheat straw was obtained from Dumor straw. Hydrochloric acid (HCl), sodium bicarbonate, and sodium hydroxide pellets (NaOH) were acquired from Fischer Scientific.

Synthesis of Silica Aerogel Precursor (SA1)

At first, 3.0 g of sodium dodecyl sulfate was dissolved in 300 mL of deionized (DI) water and agitated for 3 h at room temperature. After that, 33 mL of sodium silicate solution was added, and the solution

https://doi.org/10.1021/acsaenm.3c00664
ACS Appl. Eng. Mater. XXXX, XXX, XXX−XXX

was stirred for an additional 15 min. Subsequently, a 2 M hydrochloric acid (HCl) solution was slowly added to the mixture until the pH of the solution reached 9.0. The resulting solution was then placed in a preheated oven at 60 °C at ambient pressure overnight for gelation. For the purification of the aerogel, 1 L of DI water was added to the silica aerogel and thoroughly mixed using a mechanical agitator. The mixture was left at 60 °C at ambient pressure for 24 h. After phase separation, the upper transparent water portion was carefully removed while ensuring that the gel portion remained intact. This process was repeated twice until the water portion of the phase separation became clear, indicating complete purification.

Synthesis of Silica Aerogel Precursor (SA2)

3.0 g of SDS was dissolved in 300 mL of DI water and stirred for 1 h at room temperature. Afterward, 3 mL of mesitylene was added to the mixture and stirred for an additional 2 h. Next, 33 mL of sodium silicate solution was added, and the mixture was stirred for an additional 15 min. After that, a 2 M hydrochloric acid (HCl) solution was slowly added to the mixture until the pH of the solution reached 9.0. The gelation and purification processes are the same as before.

Synthesis of Silica Aerogel Precursor (SA3)

3.0 g of SDS was dissolved in 300 mL of DI water, and then 3 mL of mesitylene was added into it and stirred for 2 h. After that, 33 mL of sodium silicate was added, followed by the addition of 2 M hydrochloric acid to adjust the solution's pH to ∼9.0. Finally, 2.0 g of sodium bicarbonate was added to the mixture and stirred for an additional 1 h. The gelation and purification processes are the same as before.

Alkaline Treatment of Wheat Straw Fiber

Initially, 40 g of straw fiber was blended with 500 mL of DI water using a regular blender. Next, the blended fibers were poured into a beaker, and 10 g of NaOH pellets (0.5 M) was added to the solution. After the addition of NaOH, the mixture was stirred at 90 °C for 2 h. After the treatment, the fibers were filtered and washed with DI water.

Synthesis of the Cellulose–Aerogel Composite

Cellulose–aerogel gradient composites with different wt % of aerogel have been synthesized by varying aerogel concentration in the precursor mixture. Initially, the dried 0.5 M NaOH-treated straw fibers were blended with 300 mL of DI water and then mixed with the required volume of aerogel using a mechanical agitator. After that, the slurry was poured into a paper-making setup, kept between two metallic perforated sheets, and clamped using screws to maintain the thickness and prevent buckling. Finally, the as-prepared composites were dried in a preheated oven at 60 °C at ambient pressure.

Physical Measurements

The microstructure of the gradient composites was examined using a focused ion beam scanning electron microscope (FIB-SEM, Carl Zeiss AURIGA Crossbeam). Fourier-transform infrared spectroscopy (FTIR-Agilent carry 560) was employed to analyze the chemical bonding state and interfacial bonding of finely ground gradient composites. The porosity of the samples was determined using eq 1, where ρ_m represents the bulk density obtained from the ratio of weight to volume, and ρ_s indicates the skeletal density determined using the pycnometer system (Micromeritics Accu-Pyc II 1340). The equation for porosity calculation is as follows.

$$\text{Porosity}(\%) = (1 - \rho_m/\rho_s) \times 100 \quad (1)$$

Thermtest HFM-100 has been used to measure the thermal conductivity of the samples. The flexural modulus of the gradient composites was measured using a universal test system (model SSTM-20KN from United Testing Systems) for testing samples up to 500 N.

ASSOCIATED CONTENT

Supporting Information

The Supporting Information is available free of charge at https://pubs.acs.org/doi/10.1021/acsaenm.3c00664.

Image of silica aerogel (Gel form), silica aerogel powder, NaOH treated wheat straw, and gradient cellulose-aerogel composite, Image of the fabrication of gradient composite using paper making, SEM image of cellulose aerogel gradient composites, Domain and setup for the three-point bending test performed to find the elastic modulus of the material, Flexural modulus for five samples with different aerogel wt % for both the original sample and the flipped composites (PDF)

AUTHOR INFORMATION

Corresponding Author

Shenqiang Ren − *Department of Materials Science and Engineering, University of Maryland (UMD), College Park, Maryland 20742, United States;* orcid.org/0000-0002-9987-3316; Email: sren@umd.edu

Authors

Arpita Sarkar − *Department of Materials Science and Engineering, University of Maryland (UMD), College Park, Maryland 20742, United States*

Pratyush Kumar Singh − *Department of Mechanical and Aerospace Engineering, University at Buffalo, The State University of New York, Buffalo, New York 14260, United States*

Long Zhu − *Department of Materials Science and Engineering, University of Maryland (UMD), College Park, Maryland 20742, United States*

Danial Faghihi − *Department of Mechanical and Aerospace Engineering, University at Buffalo, The State University of New York, Buffalo, New York 14260, United States*

Complete contact information is available at: https://pubs.acs.org/10.1021/acsaenm.3c00664

Notes

The authors declare no competing financial interest.

ACKNOWLEDGMENTS

S.R. acknowledges the funding support on this work by the United States Department of Energy (DOE) Advanced Research Projects Agency-Energy (ARPA-E) award DE-AR0001771. D.F. and P.K.S. acknowledge the financial support from the U.S. National Science Foundation (NSF) CAREER Award CMMI-2143662.

REFERENCES

(1) Liu, L.; Zou, S.; Li, H.; Deng, L.; Bai, C.; Zhang, X.; Wang, S.; Li, N. Experimental Physical Properties of an Eco-Friendly Bio-Insulation Material Based on Wheat Straw for Buildings. *Energy Build.* **2019**, *201*, 19.

(2) Zou, S.; Li, H.; Liu, L.; Wang, S.; Zhang, X.; Zhang, G. Experimental Study on Fire Resistance Improvement of Wheat Straw Composite Insulation Materials for Buildings. *J. Build. Eng.* **2021**, *43*, 103172.

(3) Ismail, B.; Belayachi, N.; Hoxha, D. Hygric Properties of Wheat Straw Biocomposite Containing Natural Additives Intended for Thermal Insulation of Buildings. *Constr. Build. Mater.* **2022**, *317*, 126049.

(4) EPD: Straw as Insulation Material, School of Natural Building, 2021. http://schoolofnaturalbuilding.co.uk/epd-straw-as-insulation-material/ (accessed 2022-12-04).
(5) Wang, Y.; Wu, K.; Xiao, M.; Riffat, S. B.; Su, Y.; Jiang, F. Thermal Conductivity, Structure and Mechanical Properties of Konjac Glucomannan/Starch Based Aerogel Strengthened by Wheat Straw. *Carbohydr. Polym.* **2018**, *197*, 284.
(6) Wang, Y.; Zhu, H.; Tu, W.; Su, Y.; Jiang, F.; Riffat, S. Sound Absorption, Structure and Mechanical Behavior of Konjac Glucomannan-Based Aerogels with Addition of Gelatin and Wheat Straw. *Constr. Build. Mater.* **2022**, *352*, 129052.
(7) Jadhav, P. S.; Sarkar, A.; Pasupathy, S.; Ren, S. Biogenic Straw Aerogel Thermal Insulation Materials. *Adv. Eng. Mater.* **2023**, *25*, 2300037.
(8) Qi, J.; Xie, Y.; Liang, H.; Wang, Y.; Ge, T.; Song, Y.; Wang, M.; Li, Q.; Yu, H.; Fan, Z.; Liu, S.; et al. Lightweight, Flexible, Thermally-Stable, and Thermally-Insulating Aerogels Derived from Cotton Nanofibrillated Cellulose. *ACS Sustain. Chem. Eng.* **2019**, *7*, 9202.
(9) Pierre, A. C.; Pajonk, G. M. Chemistry of Aerogels and Their Applications. *Chem. Rev.* **2002**, *102*, 4243.
(10) Fricke, J.; Emmerling, A. Aerogels. *J. Am. Ceram. Soc.* **1992**, *75*, 2027.
(11) Fricke, J.; Tillotson, T. Aerogels: Production, Characterization, and Applications. *Thin Solid Films.* **1997**, *297*, 212.
(12) Su, L. F.; Miao, L.; Tanemura, S.; Xu, G. Low-Cost and Fast Synthesis of Nanoporous Silica Cryogels for Thermal Insulation Applications. *Sci. Technol. Adv. Mater.* **2012**, *13*, 035003.
(13) Ciriminna, R.; Fidalgo, A.; Pandarus, V.; Béland, F.; Ilharco, L. M.; Pagliaro, M. The Sol-Gel Route to Advanced Silica-Based Materials and Recent Applications. *Chem. Rev.* **2013**, *113*, 6592.
(14) Aegerter, M. A.; Leventis, N.; Koebel, M. M. *Aerogel Handbooks;* Springer: NewYork, 2011.
(15) Feng, J.; Zhang, C.; Feng, J.; Jiang, Y.; Zhao, N. Carbon Aerogel Composites Prepared by Ambient Drying and Using Oxidized Polyacrylonitrile Fibers as Reinforcements. *ACS Appl. Mater. Interfaces.* **2011**, *3*, 4796.
(16) Duan, G.; Jiang, S.; Jérôme, V.; Wendorff, J. H.; Fathi, A.; Uhm, J.; Altstädt, V.; Herling, M.; Breu, J.; Freitag, R.; Agarwal, S.; Greiner, A. Ultralight, Soft Polymer Sponges by Self-Assembly of short Elctrospun Fibers in Colloidal Dispersions. *Adv. Funct. Mater.* **2015**, *25*, 2850.
(17) Li, L.; Yalcin, B.; Nguyen, B. N.; Meador, M. A. B.; Cakmak, M. Flexible Nanofiber-Reinforced Aerogel (Xerogel) Synthesis, Manufacture, and Characterization. *ACS Appl. Mater. Interfaces* **2009**, *1*, 2491.
(18) Tan, J.; Maleki, P.; An, L.; Di Luigi, M.; Villa, U.; Zhou, C.; Ren, S.; Faghihi, D. A Predictive Multiphase Model of Silica Aerogels for Building Envelope Insulations. *Computational Mechanics* **2022**, *69*, 1457.

https://doi.org/10.1021/acsaenm.3c00664
ACS Appl. Eng. Mater. XXXX, XXX, XXX−XXX